The Astrophysical Journal, 735:73 (6pp), 2011 July 10 doi:10.1088/0004-637X/735/2/73

A SHELL MODEL TURBULENT DYNAMO

D. Perrone, G. Nigro, and P. Veltri
Università della Calabria, Dipartimento di Fisica and Centro Nazionale Interuniversitario Struttura della Materia, Unità di Cosenza, I-87030 Arcavacata di Rende, Italy
Received 2010 November 22; accepted 2011 April 19; published 2011 June 17

ABSTRACT

Turbulent dynamo phenomena, observed almost everywhere in astrophysical objects and also in the laboratory in the recent VKS2 experiment, are investigated using a shell model technique to describe magnetohydrodynamic turbulence. Detailed numerical simulations at very high Rossby numbers (α^2 dynamo) show that as the magnetic Reynolds number increases, the dynamo action starts working and different regimes are observed. The model, which displays different large-scale coherent behaviors corresponding to different regimes, is able to reproduce the magnetic field reversals observed both in a geomagnetic dynamo and in the VKS2 experiment. While rough quantitative estimates of typical times associated with the reversal phenomenon are consistent with paleomagnetic data, the analysis of the transition from oscillating intermittent through reversal and finally to stationary behavior shows that the nature of the reversals we observe is typical of α^2 dynamos and completely different from VKS2 reversals. Finally, the model shows that coherent behaviors can also be naturally generated inside the many-mode dynamical chaotic model, which reproduces the complexity of fluid turbulence, as described by the shell technique.

Key words: dynamo – magnetohydrodynamics (MHD) – turbulence

Online-only material: color figures

1. INTRODUCTION

The problem of magnetic dynamo, which is the amplification of a seed of a magnetic field and its maintenance against the losses of dissipation in a turbulent electrically conducting flow (Moffatt 1978), represents one of the main physical issues both in astrophysics and in geophysics. Planets, stars, and entire galaxies have associated magnetic fields and all of these fields are generated by the motion of electrically conducting fluids.

In the case of the Earth, where the mechanical energy is associated with fluid motions in the outer core, the geomagnetic field is dominated by a dipole which, as the most characteristic feature, changes its polarity from time to time. This phenomenon has been called reversals and typically lasts 10^3–10^4 years. The average time between two reversals is much longer than the duration of the reversals itself. The magnetic field of the Sun has a strong dipole component, but at lower latitudes it appears to possess a more complicated structure. Like the Earth, it changes its polarity, but periodically, with a main period of 22 years.

The difficulties faced when studying the turbulent dynamo problem are twofold: on the one hand, the huge number of degrees of freedom associated with very high values of the Reynolds numbers typical of natural turbulence does not permit direct numerical simulations even using the most powerful computing devices; on the other hand, a magneto-fluid with a Reynolds number comparable to those encountered in natural physical systems is hardly reproduced in the laboratory. Notwithstanding these difficulties, experiments—where the amplification of the magnetic field has been demonstrated in the laboratory—have been performed realizing a von Kármán flow in liquid sodium (Pétrélis et al. 2007). Recently, this experiment has been improved (VKS2 experiment), obtaining, at least locally, values of parameters larger than those corresponding to the threshold for the dynamo development. In such a way, various dynamo regimes have been observed: stationary dynamos, transitions to relaxation cycles or intermittent bursts, and random field reversals (Ravelet et al. 2008).

An efficient way to face the problem of describing the dynamical evolution of turbulent spectra at very high Reynolds numbers is furnished by the use of shell models (Frick & Sokoloff 1998; Giuliani & Carbone 1998). Some phenomenological attempts to introduce terms describing dynamo action into these models have been previously performed. In particular, Benzi (2005) considered the Gledzer-Yamada-Okhitani hydrodynamical shell model to describe the typical features of the turbulent energy cascade and introduced an ad hoc term in the first shell to impose a large-scale instability. Abrupt reversals were indeed observed at apparently random times. In the same spirit, Sorriso et al. (2007), and more recently Benzi & Pinton (2010), starting from a magnetohydrodynamic (MHD) shell model, modified the evolution equation of the first shell (second shell) for the magnetic variable b_1 (b_2), introducing a cubic interaction to reproduce the effects of the turbulent small-scale fluctuations on the largest scale (see also Nigro & Carbone 2010). Ryan & Sarson (2007) investigated the α effect of dynamo theory by coupling a low-order $\alpha\omega$-type dynamo to a shell model of fluid turbulence. In the following we attempt to set up a shell model capable of describing dynamo action without requiring any phenomenological hypothesis and remaining as close as possible to the MHD equations.

2. NUMERICAL MODEL

By decomposing the velocity $\mathbf{u}$ and magnetic field $\mathbf{b}$ into an average part ($\mathbf{u_0}$ and $\mathbf{b_0}$) varying only on large scales and a small-scale fluctuating part ($\delta\mathbf{u}$ and $\delta\mathbf{b}$) and introducing this decomposition in the MHD model, coupled dynamical equations for the average and fluctuating fields can be obtained where no assumption about the relative amplitude of the two terms has been made (Biskamp 1997). The dynamical evolution of a large-scale magnetic field can be written in the following

form:

$$\frac{\partial \mathbf{b_0}}{\partial t} = \nabla \times (\mathbf{u_0} \times \mathbf{b_0}) - \nabla \times \epsilon + \mu \nabla^2 \mathbf{b_0}, \quad (1)$$

where μ represents the magnetic diffusivity and

$$\epsilon = -\langle \delta \mathbf{u} \times \delta \mathbf{b} \rangle \quad (2)$$

is the average electric field generated by the small-scale turbulence, which describes the action of small scales on a large scale.

Let us consider an axisymmetric situation in which the large-scale velocity field is purely toroidal while the magnetic field can be decomposed into a toroidal and a poloidal component with respect to the symmetry axis; moreover, let us restrict this to local analysis in which we can approximate the toroidal ($\widehat{e_\varphi}$) and the poloidal ($\widehat{e_p}$) unit vectors with the Cartesian unit vectors $\widehat{e_x}$ and $\widehat{e_z}$, respectively. The velocity field can then be written as

$$\mathbf{u}_0 = V(y, z)\, \widehat{e_x} \quad (3)$$

and the magnetic field as

$$\mathbf{b}_0 = B_\varphi(y, z, t)\widehat{e_x} + B_p(y, t)\widehat{e_z}\,. \quad (4)$$

Let us emphasize that our fields have a dependency on two length scales: a slow scale L, which is along the y and z directions for the magnetic and velocity fields, and a fast scale k_0^{-1} along all directions (x, y, z), with the condition $k_0 L \gg 1$. These dependencies can be written explicitly as follows:

$$V = V\left(\frac{y}{L}, \frac{z}{L}, t\right), \quad B_p = B_p\left(\frac{y}{L}, t\right), \quad B_\varphi = B_\varphi\left(\frac{y}{L}, \frac{z}{L}, t\right),$$
$$\delta \mathbf{u} = \delta \mathbf{u}\left(\frac{y}{L}, \mathbf{r}, t\right), \quad \delta \mathbf{b} = \delta \mathbf{b}\left(\frac{y}{L}, \mathbf{r}, t\right), \quad (5)$$

where we can see clearly that the large-scale fields depend only on the slow scale. Projecting the evolution equation for $\mathbf{b}_0$ along $\widehat{e_x}$ and $\widehat{e_z}$, we find, respectively,

$$\frac{\partial B_\varphi}{\partial t} = \frac{\partial}{\partial z}(V B_p) + \frac{\partial \epsilon_z}{\partial y} + \mu \frac{\partial^2 B_\varphi}{\partial y^2} = \frac{\partial V}{\partial z} B_p + \frac{\partial \epsilon_z}{\partial y} + \mu \frac{\partial^2 B_\varphi}{\partial y^2} \quad (6)$$

$$\frac{\partial B_p}{\partial t} = -\frac{\partial \epsilon_x}{\partial y} + \mu \frac{\partial^2 B_p}{\partial y^2}. \quad (7)$$

In terms of the Fourier transform of the velocity ($\mathbf{u}(\mathbf{k}, t)$) and magnetic field ($\mathbf{b}(\mathbf{k}, t)$), small-scale fluctuations ϵ can also be written as

$$\epsilon = -\sum_{\mathbf{k}} \mathbf{u}(\mathbf{k}, t) \times \mathbf{b}^*(\mathbf{k}, t). \quad (8)$$

Introducing a basis in the complex physical space

$$\widehat{e_1}(\mathbf{k}), \quad \widehat{e_2}(\mathbf{k}) = \widehat{e_3}(\mathbf{k}) \times \widehat{e_1}(\mathbf{k}), \quad \widehat{e_3}(\mathbf{k}) = \frac{i\mathbf{k}}{|\mathbf{k}|} \quad (9)$$

and rewriting expression (8) in a form symmetric with respect to the change of $\mathbf{k}$ to $-\mathbf{k}$ we finally find

$$\epsilon = -\sum_{\mathbf{k}(k_z > 0)} \widehat{e_3}\, [(u_1^*\, b_2 - u_2\, b_1^*) + (u_2^*\, b_1 - u_1\, b_2^*)], \quad (10)$$

where u_1 and u_2 are the components of $\mathbf{u}(\mathbf{k}, t)$, and b_1 and b_2 are the components of $\mathbf{b}(\mathbf{k}, t)$ along $\widehat{e_1}$ and $\widehat{e_2}$, respectively. Projecting ϵ along $\widehat{e_x}$ and $\widehat{e_z}$, we find

$$\epsilon \cdot \widehat{e_x} = \epsilon_\varphi = \sum_{\frac{1}{2}\mathbf{k}\text{-space}} i \frac{k_x}{|\mathbf{k}|}\, [(u_1^*\, b_2 - u_2\, b_1^*) + (u_2^*\, b_1 - u_1\, b_2^*)], \quad (11)$$

$$\epsilon \cdot \widehat{e_z} = \epsilon_p = \sum_{\frac{1}{2}\mathbf{k}\text{-space}} i \frac{k_z}{|\mathbf{k}|}\, [(u_1^*\, b_2 - u_2\, b_1^*) + (u_2^*\, b_1 - u_1\, b_2^*)]. \quad (12)$$

Applying the Fourier transform to the dynamical evolution of velocity and magnetic field fluctuations, we can obtain the following equations:

$$\frac{\partial \mathbf{u}(\mathbf{k})}{\partial t} - i(\mathbf{k} \cdot \mathbf{b}_0)\mathbf{b}(\mathbf{k}) + \text{NLTU} + \nu k^2 \mathbf{u}(\mathbf{k}) = 0, \quad (13)$$

$$\frac{\partial \mathbf{b}(\mathbf{k})}{\partial t} - i(\mathbf{k} \cdot \mathbf{b}_0)\mathbf{u}(\mathbf{k}) + \text{NLTB} + \mu k^2 \mathbf{b}(\mathbf{k}) = 0. \quad (14)$$

In the above expressions, ν is the kinematic viscosity, while NLTU and NLTB represent, respectively, the nonlinear terms in the evolution equations for velocity and magnetic field fluctuations:

$$\text{NLTU} = -i \sum_{\mathbf{p}} M_{\mu\alpha\beta} u_\beta(\mathbf{p}, t) u_\alpha(\mathbf{k} - \mathbf{p}, t) - i \sum_{\mathbf{p}} M_{\mu\alpha\beta} b_\beta(\mathbf{p}, t) b_\alpha(\mathbf{k} - \mathbf{p}, t), \quad (15)$$

$$\text{NLTB} = -i \sum_{\mathbf{p}} M_{\mu\alpha\beta} u_\beta(\mathbf{p}, t) b_\alpha(\mathbf{k} - \mathbf{p}, t) + i \sum_{\mathbf{p}} M_{\mu\alpha\beta} b_\beta(\mathbf{p}, t) u_\alpha(\mathbf{k} - \mathbf{p}, t), \quad (16)$$

written in terms of the operator

$$M_{\mu\alpha\beta} = -\frac{1}{2}(D_{\mu\alpha} p_\beta + D_{\mu\beta} p_\alpha), \quad (17)$$

where $\mathbf{p}$ is a wavevector and $D_{\mu\alpha}$ is an orthogonal projector defined as

$$D_{\mu\alpha} = \left(\delta_{\mu\alpha} - \frac{k_\mu k_\alpha}{k^2}\right) \quad (18)$$

used to eliminate the pressure term. In Equations (13) and (14), we have estimated the spatial derivatives of the slow component as $1/L$, so that using the condition $k_o L \gg 1$ we have neglected the terms $(\mathbf{u}\cdot\nabla)\mathbf{u}_0$, $(\mathbf{b}\cdot\nabla)\mathbf{b}_0$, $(\mathbf{u}\cdot\nabla)\mathbf{b}_0$, and $(\mathbf{b}\cdot\nabla)\mathbf{u}_0$ compared to $(\mathbf{k}\cdot\mathbf{u}_0)\mathbf{u}$, $(\mathbf{k}\cdot\mathbf{b}_0)\mathbf{b}$, $(\mathbf{k}\cdot\mathbf{u}_0)\mathbf{b}$, and $(\mathbf{k}\cdot\mathbf{b}_0)\mathbf{u}$. Also, we have removed the term $i\mathbf{k}\cdot\mathbf{u}_0$ without loss of generality performing a simple Galilei's transformation (the only contribution of this term is to introduce a phase factor, $\mathbf{u} = e^{-i\mathbf{k}\cdot\mathbf{u}_0 t}\widehat{\mathbf{u}}$, in the nonlinear terms).

2.1. Shell Model

Equations (13) and (14), which describe the dynamical evolution of $\delta\mathbf{u}$ and $\delta\mathbf{b}$, display exactly the same nonlinearity as the full set of MHD equations and can be written in terms of the Fourier transform. Starting from this form, their

dynamical evolution can be described in terms of a shell model, a dynamical system (ordinary differential equations) representing a consistent and relevant way to describe the energy cascade of turbulence and to reproduce important features linked to the turbulent problem (intermittency, for example). In this model the **k**-space is divided into N concentric shells of exponentially growing radius, where the number N of shells necessary to reproduce the behavior observed at high Reynolds numbers (Re) is rather small since $N \sim \ln \mathrm{Re}$. For each shell, a scalar value $k_n = k_0\, 2^n$ of the wavevector and dynamical scalar variables $u_n(t)$ and $b_n(t)$ for the velocity and magnetic field are defined. These assigned variables (real or complex) take into account the average effects of velocity and magnetic modes between k_n and k_{n+1} and describe the chaotic dynamics of the system (Bohr et al. 1998).

A reasonable assumption is that the interactions among shells are local in k-space, since one expects that only local interactions are relevant for the energy transfer. Thus, in our shell model dynamical equations, we retain only the interactions among the neighbor and nearest neighbor shells. To explicitly derive the values of coupling coefficients in the inviscid and unforced limit the three quadratic invariants (energy, cross-helicity, and magnetic helicity) are conserved (Frick & Sokoloff 1998; Giuliani & Carbone 1998). The equations describing this model are the following:

$$\frac{du_n}{dt} = ik_n(B_\varphi + B_p)b_n - \nu k_n^2 u_n + f_n + ik_n[(u_{n+1}u_{n+2} - b_{n+1}b_{n+2}) - \frac{1}{4}(u_{n-1}u_{n+1} - b_{n-1}b_{n+1}) - \frac{1}{8}(u_{n-2}u_{n-1} - b_{n-2}b_{n-1})]^*, \quad (19)$$

$$\frac{db_n}{dt} = ik_n(B_\varphi + B_p)u_n - \mu k_n^2 b_n + ik_n\frac{1}{6}[(u_{n+1}b_{n+2} - b_{n+1}u_{n+2}) + (u_{n-1}b_{n+1} - b_{n-1}u_{n+1}) + (u_{n-2}b_{n-1} - b_{n-2}u_{n-1})]^*, \quad (20)$$

where, as usual, magnetic field components have all been divided by $\sqrt{4\pi\rho}$ (ρ being the mass density), while f_n is a hydrodynamic forcing term to inject energy into the turbulence. It is important to stress the fact that, in our model, the only forcing term is on the velocity shells. Let us finally remark that the only modification introduced in these equations, with respect to standard shell models, concerns the presence of linear terms proportional to $i(\mathbf{k}\cdot\mathbf{b}_0)$, describing the propagation of turbulent fluctuations on the large-scale magnetic field $\mathbf{b_0}$.

By rewriting the average turbulent electric field (Equation (10)) in a form consistent with the shell technique and estimating the derivative associated with the slow space dependence, as a division by the typical large-scale length L, we recast the following form of the equations for the large-scale magnetic field as:

$$\frac{dB_\varphi}{dt} = \frac{B_p V}{L} - \mu\frac{B_\varphi}{L^2} + i\sum_n \frac{1}{L}(u_n^* b_n - u_n b_n^*), \quad (21)$$

$$\frac{dB_p}{dt} = -\mu\frac{B_p}{L^2} + i\sum_n \frac{1}{L}(u_n^* b_n - u_n b_n^*). \quad (22)$$

Let us note that the expression $u_n^* b_n - u_n b_n^*$ cancels itself out in the space of wavevectors when **u** is parallel to **b** for all **k** ($u_n = \pm b_n, \forall n$). This means that nonlinear terms in Equations (21) and (22) tend to vanish when the system evolves toward a state of strong correlation between velocity and magnetic field. As the Alfvénic subspaces, characterized by $\mathbf{u}(\mathbf{r}) = \pm\mathbf{b}(\mathbf{r})$, act as attractors of the dynamics of the system (Dobrowolny et al. 1980), it is important to save this property in our model.

2.2. Numerical Parameters

The most relevant physical parameters involved in the dynamo problem are the typical large scale of slow variation, L, the typical scale of turbulent fluctuations, k_0^{-1}, the kinematic viscosity, ν, the fluid magnetic diffusivity, μ, and the rms of velocity and magnetic field fluctuations,

$$\delta u = \sqrt{\sum_n |u_n|^2}, \qquad \delta b = \sqrt{\sum_n |b_n|^2}. \quad (23)$$

For most astrophysical objects, the global rotation rate, $\omega = V/L$, also plays an important role. The relative importance of the differential rotation term can be evaluated by introducing the Rossby number, which is the ratio between the nonlinear and differential rotation terms in Equation (21):

$$\mathrm{Ro} = \frac{\delta u \delta b}{L}\frac{L}{B_p V} = \frac{\delta u}{V}\frac{\delta b}{B_p}. \quad (24)$$

When $\mathrm{Ro} \gg 1$, a condition we will assume hereafter we can neglect the differential rotation term. In such a case, the model described by Equations (19)–(22) corresponds to an α^2 dynamo and it can be seen that the poloidal and toroidal components of the large-scale magnetic field evolve in the same way, so that $B_p = B_\varphi = B$. The case $\mathrm{Ro} \ll 1$, which seems to be typical of a geodynamo, will be the object of future study.

Let us now introduce the kinematic diffusive time (τ_ν), the resistive diffusive time (τ_μ), and the eddy turnover time (τ_{NL}):

$$\tau_\nu = \left(k_0^2\nu\right)^{-1}, \quad \tau_\mu = \left(k_0^2\mu\right)^{-1}, \quad \tau_{\mathrm{NL}} = (k_0\delta u)^{-1}. \quad (25)$$

From the times above, we can calculate dimensionless numbers to characterize the turbulent behavior of our simulations:

$$\mathrm{Re} = \frac{\tau_\nu}{\tau_{\mathrm{NL}}}, \qquad R_m = \frac{\tau_\mu}{\tau_{\mathrm{NL}}}, \qquad P_m = \frac{R_m}{\mathrm{Re}}, \quad (26)$$

respectively, the Reynolds number, the magnetic Reynolds number, and the magnetic Prandtl number.

3. SIMULATIONS

We started our simulations by introducing a seed of magnetic field on a large scale when the turbulence becomes developed and stationary: i.e., we restrict the slow varying magnetic field component B to zero up to $t = 1000$. The initial conditions for shell amplitudes are $u_n = b_n = 0$, $\forall n > 3$, and $u_n(0) = 10^{-2n/3}(a + ib)$, a and b being random numbers in the interval $[-0.5, 0.5]$ and $n = 1, 2, 3$ (the shell model requires that the amplitudes of at least three modes are different from zero in order to start the simulation). The system is forced only on the shell $n = 1$ ($k_1 = k_0$) by assuming that f_1 is an exponentially correlated Gaussian noise characterized by a second moment $\langle f_1^2\rangle = \sigma^2/\ln 10$ and a correlation time τ_c, which corresponds to inject only kinetic energy at a large

scale. The shell model differential equations, Equations (19) and (20), are then integrated by using a modified fourth-order Runge–Kutta scheme. If not otherwise specified, we always fixed the separation scale such that $k_0 L = 10$, the forcing correlation time $\tau_c = 1$, and the forcing amplitude $\sigma = 9\times10^{-3}$.

At $t = 1000$, a time much longer than the eddy turnover time, the turbulence can be considered developed and is characterized by the velocity (δu) and magnetic field (δb) fluctuation levels and by their spectra. The only effect produced by varying the parameters of the forcing is to change the level of fluctuations of δu and δb. During the time evolution from $t = 0$ to $t = 1000$, the kinetic and magnetic energies grow in time and finally form a power-law spectrum. When $\tau_\mu \sim \tau_\nu$, the amplitude of magnetic and kinetic energies remain of the same order at all modes. The spectral index is close to $k^{-2/3}$ which is compatible with a Kolmogorov scaling of the second-order structure function. In contrast, as long as τ_μ decreases, δb becomes smaller compared to δu and finally, for $\tau_\mu \lesssim 10^2$ the turbulence is practically fluid (Sahoo et al. 2010). Once the turbulence developed (i.e., at $t = 1000$), we introduce a seed ($\sim10^{-10}$) on the slowly varying magnetic field components and we try to see if a dynamo effect develops. At variance with mean field MHD approximation, our model allows us to generate turbulence when a large-scale magnetic field is zero. Also, in the absence of the forcing term on the magnetic shells, the nonlinear interactions deliver energy on the magnetic variables.

4. RESULTS

The typical time evolution of the average magnetic field displays a behavior that is strongly dependent on the value of the magnetic Reynolds number R_m. Actually, the VKS2 experiment allows us to study the modification of the characteristics of dynamo magnetic field time evolution as a function of the magnetic Reynolds number (the change in R_m corresponds to the rotation of the impellers at different speeds; Ravelet et al. 2008). For this reason we have performed different sets of simulations: in each of them, we have fixed the value of τ_ν and we have let τ_μ vary between 1 and τ_ν. In any of these simulation sets, we have verified the same phenomenology as a function of τ_μ: increasing the value of τ_μ, we obtain different dynamical behaviors for B.

As can be seen in Figure 1, under a threshold value of R_m, the turbulence is not capable of generating a dynamo effect. We observe that the zoom in Figure 1 displays a discontinuity in slope in the vicinity of R_{mc} analogous to some response functions at phase transitions or bifurcations in the presence of noise. When R_m increases ($\tau_\mu \approx 10^3$), the large-scale magnetic field displays a behavior characterized by very low amplitude intermittent bursts of oscillations (see Figure 2(a)). Moreover, fluctuating magnetic energy is an order of magnitude smaller than the kinetic one. Increasing R_m, the system endures a new bifurcation and a new dynamical behavior appears in which it displays irregular oscillations. A further increase of R_m (τ_μ up to $\approx10^5$) gives rise to turbulent magnetic and kinetic fluctuations more or less of the same order, while the dynamo magnetic field displays a series of reversals between two opposite sign magnetic field levels (see Figure 2(c)). Finally, when $\tau_\mu \geqslant 10^5$ we observe that the magnetic field saturates to a stable level. After the initial growth the level of the magnetic field does not change anymore. Some fluctuations on the magnetic field still remain but they are centered around the stable level (see Figure 2(d)). As a consequence, reversals are observed in a finite interval range, in particular for Re $\simeq 10^7$ and $10^3 < R_m < 10^5$.

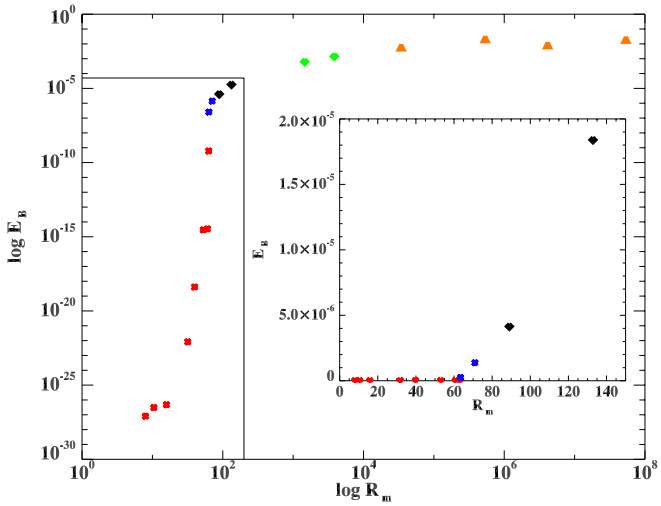

Figure 1. Dynamo magnetic field energy (E_B) as a function of the magnetic Reynolds number (R_m) in the log–log scale for Re $\simeq 10^7$. Note that the magnetic field saturates for a high magnetic Reynolds number. Legend: no dynamo (red crosses); oscillating intermittent dynamo (blue crosses); irregularly oscillating behavior (black diamonds); magnetic reversals (green diamonds); stationary dynamo (orange triangles). The dashed line indicates the threshold region, zoomed in the inset in linear scale.

(A color version of this figure is available in the online journal.)

These figures are reproduced in the VKS experiment (Ravelet et al. 2008), where reversals also exist inside a finite interval range of parameters.

It is worth noting that in any case the large-scale magnetic field energy level is always lower than or, at best, of the same order as the kinetic energy level of fluctuations. This means that there is a tendency to realize a sort of equipartition between fluctuating kinetic energy and dynamo magnetic energy. There is no stage of the dynamical evolution where the energy of fluctuations is smaller than the energy of the magnetic field; this suggests that it is not possible to describe the phenomenon by using a linear or quasi-linear approximation.

In order to understand the nature of the transitions between the different regimes, we have also represented in Figure 3 the dynamic evolution of the large-scale magnetic field in phase space $[B(t), B(t+\tau) - B(t)]$. It can be seen that at variance with the behavior of the VKS experiment, where robust trajectories exist in such phase space due to the presence of four fixed points (Ravelet et al. 2008), in our case the trajectories change drastically from one regime to the other. In relation with this change, the rms of the large-scale magnetic field becomes higher when reducing magnetic diffusivity. Moreover, in our simulations the transition from reversal to stationary dynamo occurs in the opposite way with respect to the VKS experiment. The apparently counter-intuitive fact that a higher R_m value leads finally to a more regular dynamo (via the transition oscillatory–reversal–stationary) seems to be a generic feature of an α^2 dynamo (Stefani & Gerbeth 2005) and is perhaps due to the fact that the fixed points of Equation (22) depend on the magnetic diffusivity which represents the order parameter of the transitions. In contrast, in the VKS experiment the stability of the fixed points is guaranteed by the existence of two dynamos with opposite signs (Pétrélis & Fauve 2008; Pétrélis et al. 2009; Gissinger et al. 2010; Gissinger 2010).

Let us now discuss the reversal regime in more detail. In Figure 2(c), it is seen that the time between two reversals is much longer than typical timescales of turbulence. This corresponds

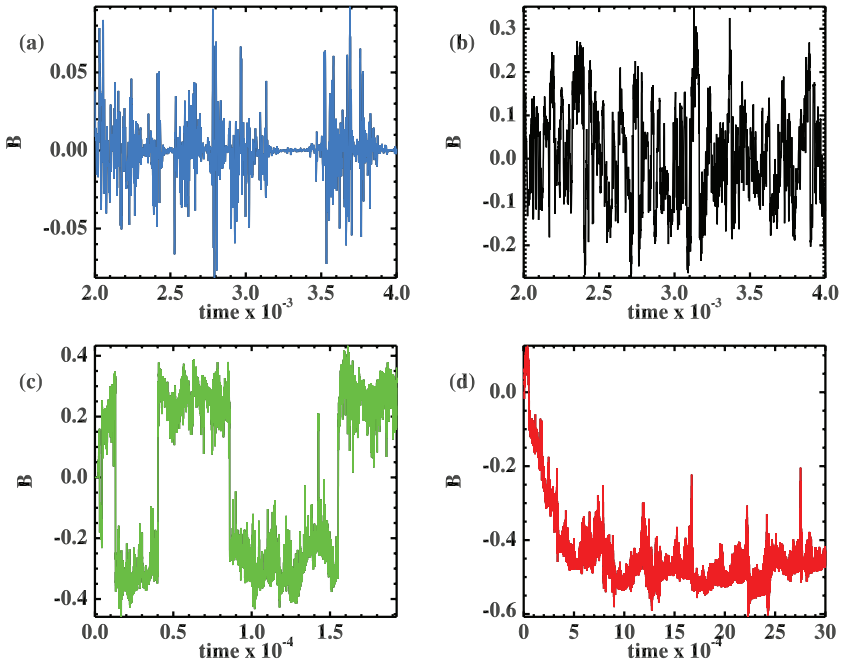

Figure 2. Time evolution of the large-scale magnetic field in dimensionless unit (time is normalized to τ_{NL}, while B is normalized to δu). (a) Oscillating intermittent dynamo for Re $\simeq 7.6 \times 10^6$ and $R_m \simeq 62$. (b) Irregularly oscillating behavior for Re $\simeq 6.5 \times 10^6$ and $R_m \simeq 129$. (c) A series of reversals for Re $\simeq 1.9 \times 10^7$ and $R_m \simeq 3.9 \times 10^3$. (d) Stationary dynamo for Re $\simeq 5.4 \times 10^7$ and $R_m \simeq 5.4 \times 10^5$.

(A color version of this figure is available in the online journal.)

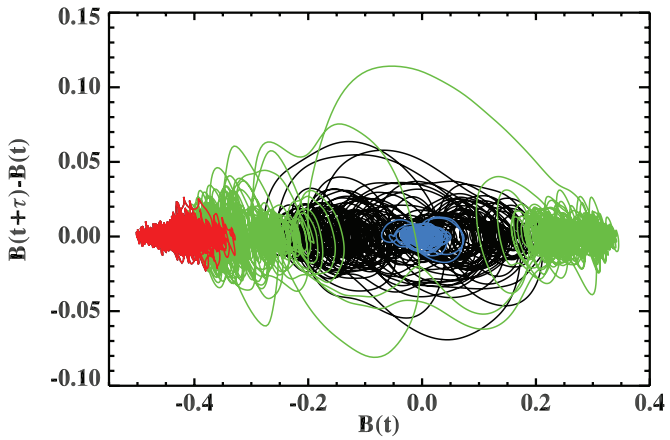

Figure 3. Dynamic evolution of large-scale magnetic field in the phase space $[B(t),\ B(t+\tau) - B(t)]$ for the different regimes observed. Blue: oscillating intermittent dynamo ($\tau \simeq 0.25$). Black: irregularly oscillating behavior ($\tau \simeq 0.22$). Green: reversals ($\tau \simeq 0.66$). Red: stationary dynamo ($\tau \simeq 1.76$). The parameter is the same as in Figure 2.

(A color version of this figure is available in the online journal.)

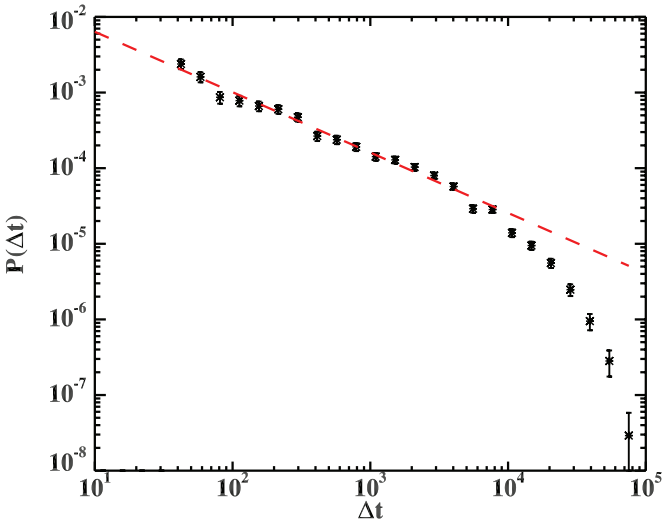

Figure 4. Probability distribution function for reversal waiting times, in the log–log scale, where $k_0 L = 5$, Re $\simeq 4.5 \times 10^7$, and $R_m \simeq 9.1 \times 10^4$. The red dashed line represents the slope of power-law linear fit: $\log P(\Delta t) = m \log \Delta t + C$, with $m = -0.8$.

(A color version of this figure is available in the online journal.)

to what happens both in Earth magnetic field reversals (Sorriso et al. 2007; $\tau_{NL} \sim 10^3$ yr) and in the VKS2 experiment (Ravelet et al. 2008; $\tau_{NL} \sim 0.05$ s). The reversals are abrupt. The time necessary to reverse the magnetic field, i.e., the time required to move from one level to another of the magnetic field is of the order of $\sim\tau_{NL}$. Also in a geodynamo and the VKS experiment, the reversals are fast events: in Earth's case the reversal times are of the order of some kyr, while in the experiment ~4–5 s, which, at variance with our simulations, is 10^2 longer than the nonlinear time (of the order of the diffusive time). Figure 2(c) also shows another important phenomenon related to the magnetic reversals—the excursions. The polarity begins to change; instead of executing a full transition, the dipole returns to the original polarity. The same features exist in a geodynamo.

The sequence of the reversals displays a behavior which seems to be the result of a chaotic (or stochastic) process. To characterize such a complex process we performed a statistical analysis by running a very long simulation, and by calculating the probability distribution function (PDF) of the waiting times, i.e., the times between two consecutive reversals. The obtained distribution is reported in Figure 4, in a log–log scale. It is clearly seen that over more than two decades it displays a power-law behavior, which is the signature of a non-Poisson process. In other words, the phenomenon of magnetic field reversals is

not purely stochastic, but it is characterized by memory effects due to the presence of long-range correlation. This behavior is also characteristic of Earth magnetic field reversals (Sorriso et al. 2007). For very long waiting times, the PDF displays exponentially decreasing behavior.

5. CONCLUSIONS

In the case of the very high value of Rossby number we studied, our model mimics a developed MHD turbulence and its corresponding large-scale α^2-type dynamo effect. The time evolution of the large-scale magnetic field is characterized by different regimes of coherent behaviors which are determined by the nonlinear interaction of the dynamical variables of turbulence, which in turn display a chaotic behavior. It has been suggested that the different coherent dynamical behaviors observed can be produced by the nonlinear interaction of a few modes (Rikitake 1958). Indeed, models of the Rikitake type (Rikitake 1958) seem to be able to reproduce some of these coherent behaviors. We think that it is extremely relevant to show that these behaviors can be generated also inside a many-mode dynamical chaotic model, which reproduces a complex physical system of MHD turbulence like that described by the shell technique.

REFERENCES

Benzi, R. 2005, Phys. Rev. Lett., 95, 024502
Benzi, R., & Pinton, J.-F. 2010, Phys. Rev. Lett., 105, 024501
Biskamp, D. 1997, Nonlinear Magnetohydrodynamics (Cambridge: Cambridge Univ. Press)
Bohr, T., Jensen, M. H., Paladin, G., & Vulpiani, A. 1998, Dynamical Systems Approach to Turbulence (Cambridge: Cambridge Univ. Press)
Dobrowolny, M., Mangeney, A., & Veltri, P. 1980, Phys. Rev. Lett., 45, 144
Frick, P., & Sokoloff, D. 1998, Phys. Rev. E, 57, 4155
Gissinger, C. 2010, Phys. Rev. E, 82, 056302
Gissinger, C., Dormy, E., & Fauve, S. 2010, Europhys. Lett., 90, 49001
Giuliani, P., & Carbone, V. 1998, Europhys. Lett., 43, 527
Moffatt, H. K. 1978, Magnetic Field Generation in Electrically Conducting Fluids (Cambridge: Cambridge Univ. Press)
Nigro, G., & Carbone, V. 2010, Phys. Rev. E, 82, 016313
Pétrélis, F., & Fauve, S. 2008, J. Phys.: Condens. Matter, 20, 494203
Pétrélis, F., Fauve, S., Dormy, E., & Valet, J.-P. 2009, Phys. Rev. Lett., 102, 144503
Pétrélis, F., Mordant, N., & Fauve, S. 2007, Geophys. Astrophys. Fluid Dyn., 101, 289
Ravelet, F., et al. 2008, Phys. Rev. Lett., 101, 074502
Rikitake, T. 1958, Proc. Camb. Phil. Soc., 54, 89
Ryan, D. A., & Sarson, G. R. 2007, Geophys. Res. Lett., 34, L02307
Sahoo, G., Mitra, D., & Pandit, R. 2010, Phys. Rev. E, 81, 036317
Sorriso-Valvo, L., Stefani, F., Carbone, V., Nigro, G., Lepreti, F., Vecchio, A., & Veltri, P. 2007, Phys. Earth Planet. Inter., 164, 197
Stefani, F., & Gerbeth, G. 2005, Phys. Rev. Lett., 94, 184506